INSTITUTE OF PHYSICS PUBLISHING SUPERCONDUCTOR SCIENCE AND TECHNOLOGY
Supercond. Sci. Technol. **19** (2006) 1233–1239 doi:10.1088/0953-2048/19/12/002

Size effects on the magnetic properties of Cu–Nb nanofilamentary wires processed by severe plastic deformation

M J R Sandim[1], D Stamopoulos[2], H R Z Sandim[1], L Ghivelder[3], L Thilly[4], V Vidal[4,5], F Lecouturier[5] and D Raabe[6]

[1] Escola de Engenharia de Lorena, Universidade de São Paulo, Lorena 12600-970, SP, Brazil
[2] Institute of Materials Science, NCSR 'Demokritos', 153-10, Aghia Paraskevi, Athens, Greece
[3] Instituto de Física, Universidade Federal do Rio de Janeiro, Rio de Janeiro 21945-970, RJ, Brazil
[4] Laboratoire de Métallurgie Physique, Université de Poitiers, SP2M1, 86960 Futuroscope, France
[5] Laboratoire National des Champs Magnétiques Pulses, CNRS-UPS-INSA, 31400 Toulouse, France
[6] Max-Planck-Institut für Eisenforschung, D-40237, Düsseldorf, Germany

Received 4 September 2006, in final form 28 September 2006
Published 23 October 2006
Online at stacks.iop.org/SUST/19/1233

Abstract
We report on the influence of the microstructure on the AC and DC magnetic properties of Cu–3.5% Nb nanofilamentary wires. Samples obtained from a single Cu–3.5% Nb wire were subsequently submitted to different plastic strain levels via drawing so that their microstructure was altered. Noticeable differences are observed in their isothermal DC magnetization curves that present a double-peak structure. The first peak, which occurs at low magnetic fields, is attributed to superconductivity induced in the Cu matrix due to the proximity effect. It is argued that the second peak is related exclusively to niobium. The dependence of these two distinct peaks on the characteristic nanometre length scales of the samples, i.e. dimension of the Nb filaments and interfilamentary spacing, are discussed.

1. Introduction

Multifilamentary Cu–Nb composites exhibit high strength and good electrical conductivity [1, 2]. Due to the combination of such properties, these materials are attractive for the design of high-field magnets [3, 4]. Indeed, the generation of high pulsed magnetic fields by non-destructive magnets (over 70 T) requires winding materials with extreme properties which are difficult to achieve with usual single-phase materials and *microcomposites* [4, 5]. Therefore, one possible solution consists in developing Cu–Nb composites with Nb filaments in the *nanometre* range [4, 5]. Due to the size reduction of the reinforcing phase, such materials have indeed unique and interesting physical properties: the tensile strength of the Cu–Nb nanocomposites is very high, up to 2 GPa at 77 K, much greater than predicted from the classical rule of mixtures for coarse-grained samples of the same composition [5, 6]. Another important feature of such materials concerns the solid state interdiffusion observed after severe plastic deformation [7, 8]: although the solubility of Cu and Nb is known to be negligible in the equilibrium state, some intermixing between Cu and Nb atoms at Cu–Nb interfaces (amorphous zones) was observed as a result of severe plastic deformation [7–9].

It is also known that the amount of internal phase boundaries and the filament spacing play a fundamental role in both mechanical [5, 8] and normal state electrical properties of Cu–Nb composites [10, 11]. The superconducting properties of Cu–Nb multifilamentary wires, mainly obtained from transport measurements, have also been reported in several works [12–16]. Moreover, in agreement with previous studies, magnetization measurements can serve as a sensitive probe that unveils the interfaces' structural quality in Cu–Nb composites [16–19]. These magnetization studies [16–19] were performed using Cu–Nb composite wires with coarse

Nb filaments with typical dimensions in the *micrometre* range, focusing on the influence of thermal instability mechanisms on their microstructure and eventually on their superconducting properties [16–19].

In the present work we focus on the size effects on the magnetic properties of Cu–Nb multifilamentary wires with both dimensions of the niobium filaments and their interfilamentary spacing in the *nanometre* range, typically below 10 nm. These nanocomposite wires were processed by the bundle and draw technique for the winding of high pulsed resistive magnets [4, 5].

During the manufacture of multifilamentary Cu–Nb wires (via series of cold drawing steps), the initial rod-like niobium filaments generally develop a ribbon-like shape with increasing drawing strain. This phenomenon arises to a larger extent in the so-called '*in situ*' composites obtained from an arc-melted Cu–Nb mixture [8] compared to 'continuous' composites obtained from the bundle and draw technique applied on a bulk Cu–Nb billet. However, even in continuous wires this phenomenon cannot be avoided. After extreme plastic deformation the Nb filaments develop a curled morphology which can be observed in the cross-section of the wire [9]. In spite of this striking feature of the niobium filaments, the geometry of those materials with both niobium filaments and interfilamentary spacing in the nanometre scale is quite similar to that of a superconductor with a multilayer structure [20–22].

The investigation of the superconducting composite conductors, including those with normal metal matrix, is still a subject of interest [23]. Due to their peculiar characteristics, the study of the influence of the interfaces on the physical properties of Cu–Nb nanocomposite wires is valuable not only for practical applications, but also for understanding the fundamental issues related to other heterogeneous superconducting systems. Therefore in this paper, after a brief description of the elaboration process of multifilamentary Cu–Nb nanocomposites, we report on some microstructural studies via field emission gun scanning electron microscopy and electron back scattering diffraction. Then the magnetic properties in the superconducting state are presented. Finally, we relate these properties to the microstructural state and to the Cu–Nb interfaces structure.

2. Experimental details

The elaboration process of the investigated nanocomposites with nominal composition of Cu–3.5% Nb is based on severe plastic deformation applied by repeated series of hot extrusion and cold drawing steps [5]: a Nb rod is inserted into a Cu jacket, called Cu-0; after a hot-extrusion stage, the billet is cold drawn to an hexagonal shape. 85 ($=N$) segments of this wire are bundled and inserted into a Cu jacket, called Cu-1. The series of hot extrusion/cold drawing/bundling is iterated five times to obtain 85^5 ($=4.4 \times 10^9$) continuous Nb nanofilaments embedded in the multiscale Cu matrix, distributed over the interfilamentary Cu (Cu-0), and the Cu-i channels ($i = 1, \ldots, 5$) surrounding groups of N^i niobium filaments. In the present work we study three samples of Cu–3.5% Nb, labelled A1, A2 and A3, whose main characteristics are displayed in table 1.

Table 1. Characteristics of the Cu–3.5% Nb nanocomposite wires containing 85^5 Nb nanofibres: d, d_{Nb}, d_{Cu-0} and RA are defined in the text.

Cu–3.5% Nb	d (mm)	d_{Nb} (nm)	d_{Cu-0} (nm)	RA (%)
A1	2.416	6.7	1.2	88.71
A2	1.985	5.5	1	92.38
A3	1.571	4.4	0.8	95.23

All the samples were obtained from a conductor containing 85^5 Nb filaments with diameter 7.19 mm obtained after severe plastic deformation to a total true strain $\eta = \ln(A_0/A) \approx 29$, where A is the final cross-section and A_0 the initial cross-section of the first billet. This wire was annealed at 973 K for 60 min. After this recrystallization heat treatment, the conductor was cold drawn to different final diameters: $d =$ 2.416, 1.985, 1.571 mm for A1, A2, A3 samples respectively, with the corresponding reduction in area $\mathrm{RA} = (A_i - A)/A_i =$ 88.71%, 92.38%, 95.23% respectively (A_i is the cross-section at the previous annealing stage, i.e. at $d = 7.19$ mm here). Table 1 displays the theoretical values for the diameter of the niobium filaments (d_{Nb}) and the interfilamentary spacing d_{Cu-0}: d_{Nb} is below 10 nm, while d_{Cu-0} is smaller than 2 nm. Therefore, the essential difference between the samples is the amount of applied cold drawing strain and the resulting microstructure size.

The microstructure of the Cu/Nb nanocomposites was investigated by means of JEOL JSM-6500F and Zeiss XB1560 field emission gun microscopes in the secondary electrons mode. The microtexture was determined by means of automated acquisition and indexing of Kikuchi patterns after suitable image processing in a TSL system (provided by TexSem Laboratories) interfaced to a JEOL JSM-6500F field emission gun scanning electron microscope (FEG-SEM) operating at 15 kV. Electron backscatter diffraction (EBSD) sampling points were made with a step size of 50 nm. (110)-pole figures and grain boundary characteristics were determined for each mapped region. The magnetization measurements were performed using a physical property measurement system (PPMS) and a SQUID magnetometer (both Quantum Design). The samples were 15 mm long and the external magnetic field was applied parallel to the wire axis. DC magnetization measurements as a function of magnetic field, $M(H)$, were performed at several temperatures in the range $3\ \mathrm{K} \leqslant T \leqslant 7\ \mathrm{K}$ and with magnetic fields up to 2 T. The temperature dependence of the real part of the AC magnetic susceptibility, $\chi'(T)$, was determined from 3 to 12 K. The applied AC magnetic field amplitude was 1 Oe with a frequency of 50 Hz.

3. Results and discussion

3.1. Microstructural characterization

Representative SEM images of the cross-section of the Cu–3.5% Nb nanocomposites (containing 85^5 Nb fibres) are shown in figures 1(a)–(d). These images refer to the sample A2. Figure 1(a) shows a bundle containing 85^4 niobium filaments. The full cross-section of the conductor contains 85 of such cells. Each cell is composed of 85 structures with 85^3 niobium filaments each. One specific structure is enlarged

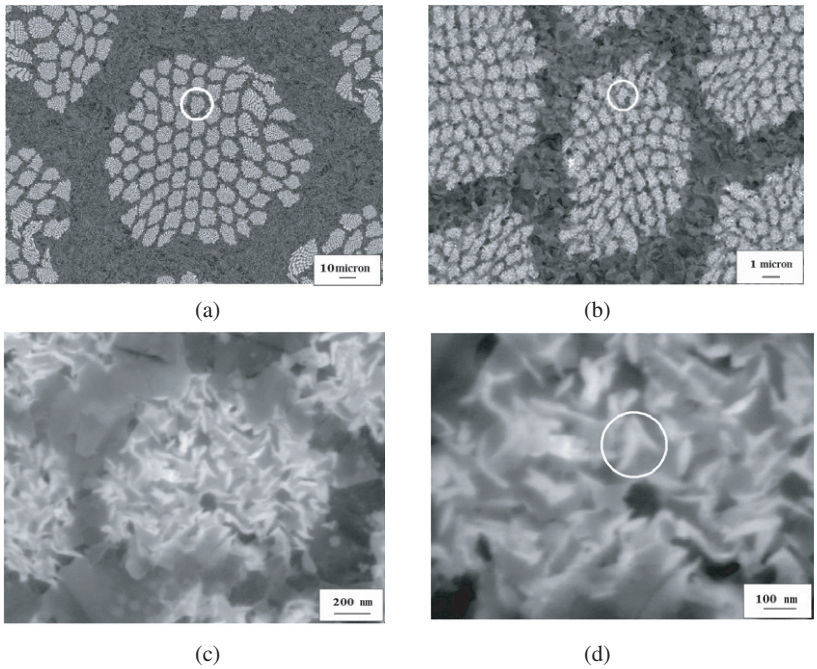

Figure 1. High-resolution SEM micrographs showing the cross-section of the Cu–3.5% Nb nanocomposite wire (sample A2): (a) a cell containing 85^4 niobium filaments is shown in the central part of the image; the marked area is enlarged in the next micrograph; (b) structure containing 85^3 niobium filaments; the marked area is enlarged in the next image; (c) bundle composed of 85^2 niobium filaments; (d) the image of the same bundle depicted at larger magnification. The marked area contains 85 niobium filaments.

in figure 1(b). In this figure, the bundle marked with a circle contains 85^2 niobium filaments. This bundle is further magnified in figures 1(c) and (d). In figure 1(d), the encircled zone is supposed to contain 85 niobium filaments. In this picture, individual filaments cannot be resolved from interfilamentary Cu channels (Cu-0) because their nanometre size is smaller than the resolution provided by the scanning electron microscope.

Figure 2 depicts the results of high-resolution EBSD measurements performed on sample A2. The partition of the EBSD data allows one to get the microtextures corresponding to Nb and Cu phases. The Cu matrix has two major orientation components ⟨111⟩ and ⟨100⟩ in the wire axis direction. Previous work [24, 25] has shown that this duplex texture arises from a balance between energy storage during severe plastic deformation (build-up of dislocation substructures transforming into fine ⟨111⟩ grains via dynamic recovery) and energy release during recrystallization heat treatment (nucleation of ⟨200⟩ grains at high angle boundaries and growth via grain boundary migration). In spite of their small volume fraction (3.5%), the Nb filaments could be detected: they exhibit a ⟨110⟩-fibre texture in the wire axis direction, as observed in coarser structures [26]. The presence of a sharp ⟨110⟩-fibre texture in the Nb filaments when embedded in a ⟨111⟩ Cu matrix leads to the development of curled structures [8, 9]. Grains bend around one another to satisfy the strain compatibility of neighbouring grains [26]. Figures 1 and 2 show this curling effect in the Nb filaments clearly. In this sense, it must be stressed that the values of d_{Nb}, the nominal diameter of each Nb filament, and $d_{\mathrm{Cu-0}}$, the nominal Cu thickness between two adjacent Nb filament, displayed

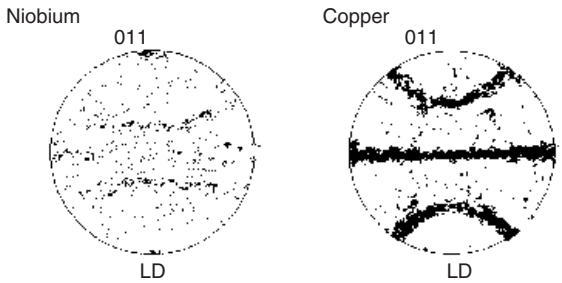

Figure 2. {110} discrete pole figures corresponding to the Cu–3.5% Nb nanocomposite wire (sample A2). LD is the longitudinal direction of the wire, i.e. perpendicular to the wire axis.

in table 1 are theoretical mean values. Based on the high-resolution SEM images shown in figure 1 one expects the presence of some distribution of real dimensions in the entire multifilamentary arrangement.

3.2. Magnetic characterization

Figure 3 shows the temperature dependence of the real (χ') part of the AC magnetic susceptibility for the investigated samples. The superconducting critical temperature (T_c) is 8.1 K for sample A1 (for pure bulk Nb, $T_c = 9.2$ K). There is no significant difference between the T_c values for the others samples: T_c is found to be approximately 7.8 K. However, at low temperatures it is clearly observed that the diamagnetic signal is more pronounced for sample A3. This indicates a stronger proximity coupling between the niobium filaments in the most drawn sample.

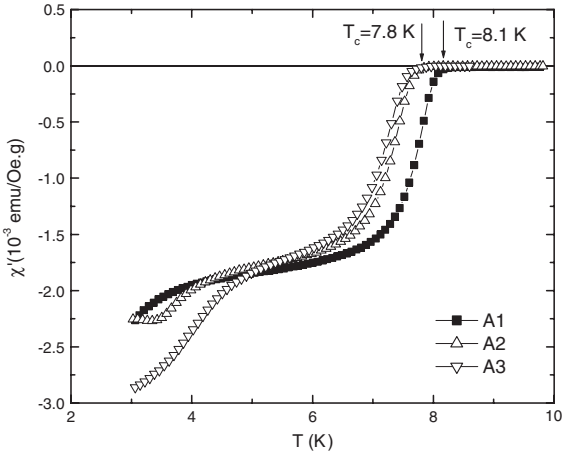

Figure 3. Temperature dependence of the real part of the AC magnetic susceptibility, χ', for the Cu–3.5% Nb nanocomposite wires ($N = 85^5$ Nb nanofibres).

A deeper understanding of the influence of the microstructure, which is modulated by the applied strain, on the superconducting properties of the Cu–3.5% Nb may be obtained from the DC magnetic characterization. Figure 4(a) shows representative isothermal magnetization curves, $M(H)$, for sample A2. A noticeable characteristic of these curves is that, for increasing field, in addition to the first peak H_{fp} that occurs for low magnetic fields, a second distinct peak appears at a characteristic field H_{sp}. This double-peak structure is nicely illustrated in figure 4(b), which displays only the ascending branches of the $M(H)$ curves at several temperatures in the range 3 K $< T <$ 7 K. Such a feature is also found in the magnetization curves for the other investigated samples (data not shown). The temperature dependence of the first and second peaks' position as well as the upper critical field (H_{c2}) is shown in figure 5, in which all the characteristic data are presented in an H–T diagram. From the DC magnetization data, valuable information concerning the size effects of the Cu–3.5% Nb nanocomposite wires are obtained, which are discussed in the following paragraphs.

3.2.1. Dimensional effects. At zero temperature, the Ginzburg–Landau coherence length of the investigated samples is $\xi(0) \sim 15$ nm, as estimated from the standard Ginzburg–Landau theoretical expression $H_{c2}(0) = \Phi_0/2\pi\,\xi^2(0)$ (the extrapolation of the upper critical field lines presented in figure 5 down to zero temperature gives 18 kOe $< H_{c2}(0) <$ 21 kOe). Therefore, for all temperatures $T < T_c$ the following conditions hold: (i) $\xi(T) \gg d_{Nb}$ and (ii) the interfilamentary spacing is even smaller than each Nb filament, $d_{Nb} > d_{Cu}$ (see table 1). Consequently, for $T < T_c$ the electrons forming a Cooper pair are spatially separated over many niobium filaments, and it is expected that the system should behave nearly as a bulk superconductor. Such argumentation is supported by the temperature dependence of $H_{c2}(T)$ shown in figure 5. The upper critical field is very sensitive to the coupling between the superconducting filaments, since $H_{c2} \propto 1/\xi^2(T)$. In the investigated system, both the niobium filaments and the interfilamentary spacing are in the *nanometre* scale. So, in spite of the curling of the

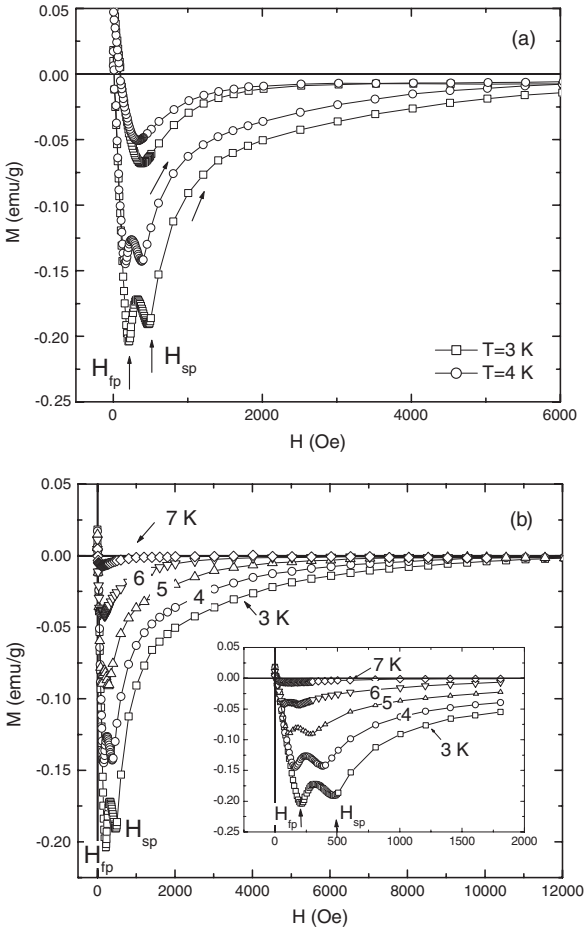

Figure 4. DC magnetization curves for the Cu–3.5% Nb nanocomposite wire (sample A2): (a) ascending (indicated by arrows) and descending branches of the $M(H)$ curves at $T = 3$ and 4 K; (b) ascending branches of $M(H)$ curves for $T = 3$, 4, 5, 6, and 7 K, which are displayed in a different scale in the inset.

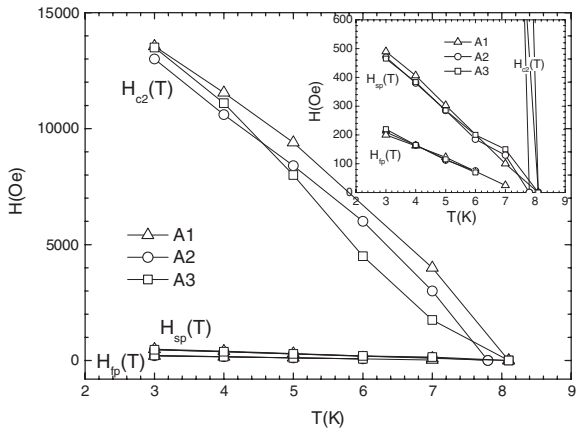

Figure 5. Characteristic field lines $H_{c2}(T)$, $H_{fp}(T)$ and $H_{sp}(T)$ for the investigated Cu–3.5% Nb nanocomposite samples.

niobium filaments it is interesting to compare the temperature dependence of $H_{c2}(T)$ with that predicted for superconducting multilayers [20–22]. Figure 6 displays the log–log plot of the $(T - T_c)$ dependence of the upper critical field for the

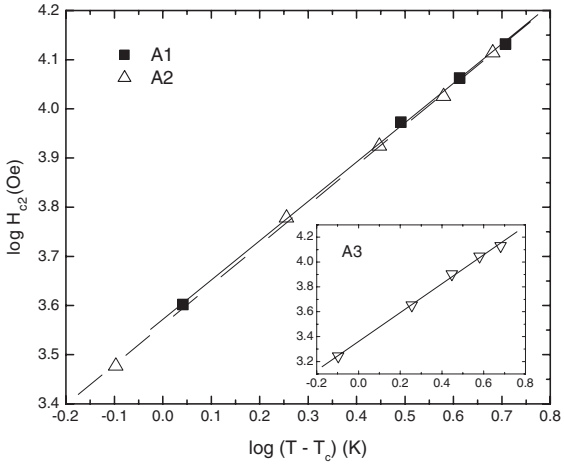

Figure 6. Log–log plot of the upper critical magnetic field, H_{c2}. The continuous and segmented lines are the linear fits of the data concerning two samples A1 and A2, respectively. Results for sample A3 are displayed in the inset.

Cu–Nb nanocomposite wires. From this figure it is observed that $H_{c2}(T)$ can be described by $H_{c2}(T) \propto (T - T_c)^f$ for $T < T_c$. In addition, it is found that $f = 0.8$ for samples A1 and A2 and $f = 1.1$ for the most deformed sample, A3 (see the inset of figure 6). The obtained f values indicate that the $(T - T_c)$ dependence of $H_{c2}(T)$ is almost linear for all investigated samples, a characteristic of three-dimensional superconducting systems [20–22].

3.2.2. Double-peak structure in the magnetization curves. From the H–T diagram displayed in figure 5 there are no major differences concerning the temperature dependence of the first (H_{fp}) and second (H_{sp}) peaks' position of the investigated samples. However, the absolute magnetization values at H_{fp} and H_{sp} reveal interesting differences between the samples, specifically related to their characteristic length scales d_{Nb} and d_{Cu-0}. Figure 7 shows the double-peak structure in the $M(H)$ curves at $T = 3$ and 4 K for all samples. It is interesting to note that the magnitude of the first and second peaks has an opposite behaviour with respect to the reduction of the interfilament spacing, d_{Cu-0}, and the dimension of Nb filaments, d_{Nb}, respectively. Previous studies on multifilamentary wires with characteristic dimensions in the *micrometre* range [17–19] clearly proved that the distinct peak observed at low magnetic fields is due to proximity coupling. In the present samples with characteristic dimensions in the *nanometre* range, when the conductor's diameter decreases the interfilament spacing d_{Cu-0} decreases as well (see table 1). The proximity effect is then expected to become more pronounced, as indeed observed in figure 7: the first peak magnitude clearly increases as d_{Cu-0} decreases. In contrast, in figure 7 we clearly see that as the dimension of Nb filaments, d_{Nb}, decreases (see table 1) the second peak is gradually suppressed. For sample A3 only a slight change in the slope of the $M(H)$ curve is observed. At this point of the discussion it must be stressed that there is storage of geometrically necessary dislocations at the Cu–Nb interfaces [27] because of the lattice parameter difference between the face-centred cubic (fcc) and the body-centred cubic (bcc) phases, respectively Cu and Nb [27]. Such

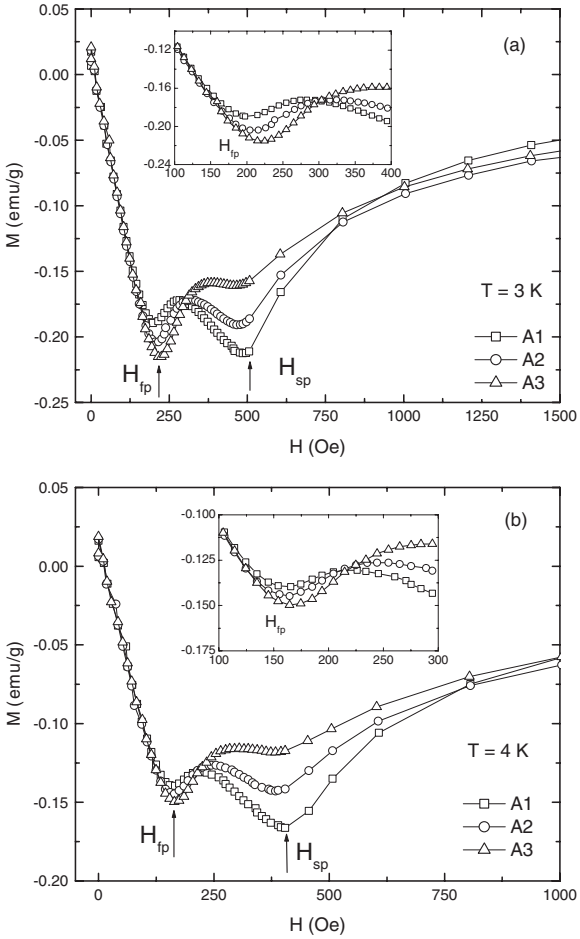

Figure 7. Ascending branches of the $M(H)$ curves at (a) 3 K and (b) 4 K for the Cu–3.5% Nb nanocomposite wires. The inset shows details of the curves for low magnetic fields.

misfit dislocations at the interfaces of Cu–Nb nanocomposites have been characterized, for example, using high-resolution TEM [7, 28]. Coming back to figure 7, the behaviour of the second peak may be explained by recalling that the Cooper pairs need a spatial separation of the order of $\xi(T)$ in order to be formed without being scattered and eventually destroyed by any kind of structural imperfection. Thus, as the dimension of Nb filaments, d_{Nb}, gets smaller the Cooper pairs that were originally hosted in each filament are now scattered by a great number of structural imperfections that they experience at the Nb–Cu interfaces. It is then expected that the second peak, H_{sp}, related to the in-filament superconducting condensate is suppressed as d_{Nb} decreases. This is indeed observed in the data presented in figure 7. In this context it seems that the superconducting condensate redistributes from the in-filament Nb areas to the interfilamentary Cu matrix regimes as the characteristic length d_{Nb} and d_{Cu-0} are decreased down to the nanometre range. The proposed explanation is, of course, only phenomenological. In particular, it does not take into account the fact that the zero-temperature coherence length, $\xi(0)$ around 15 nm, is already higher than the dimension of Nb filaments. Obviously, a more sophisticated model is needed in order to explain consistently all the aspects of the data.

Except for the pair breaking that occurs at the Nb–Cu interfaces, there are two other factors that could influence the evolution of the double-peak structure.

(i) The pair breaking that occurs *inside* the Nb filaments. Heavy scattering by extended structural imperfections inside the Nb filaments could also result in pronounced pair breaking. Since the applied drawing strain is higher for sample A3 we may also assume that this sample is more disordered and consequently the in-filament superconducting condensate should be more suppressed when compared to samples A2 and A1. However, a puzzling question is to understand the origin of such disorder, since the storage of dislocations *inside* the nanometre-scale Nb filaments is expected to be strongly reduced (and even suppressed) compared to micrometre-scale filaments, as a result of a size effect on the plasticity mechanisms [5]. Thus, if the suppression of the second magnetization peak, observed in the data presented in figure 7, is also due to the plastic strain induced in the samples during their preparation, it appears difficult to relate it to traditional 'in-volume' dislocation storage.

(ii) The morphology/structure of the Cu–Nb interfaces changes owing to severe plastic deformation. In particular, after a total true strain greater than 30 (sample A3), one could expect some structurally distorted Cu–Nb interfaces by mechanical alloying as observed on much less deformed Cu–Nb nanocomposites [7–9]. In thermodynamical equilibrium the intersolubility of Cu and Nb is known to be negligible at all temperatures, while no compounds or intermediate phases occur in the Cu–Nb system. Therefore, the origin of such Cu–Nb mixed zones at the interfaces in the form of crystalline or amorphous alloy was related to the large strains [7–9]. Indeed, the reduction of microstructure via repeated drawing is accompanied with a strong increase of the area of Cu–Nb interfaces, i.e. with an increase of the internal energy of the Cu–Nb system. Hence, the thermodynamical equilibrium may be changed, and the intersolubility of Cu–Nb modified. To reduce the stored internal energy, some interdiffusion may be promoted by the motion of dislocations and vacancies produced during the severe plastic deformation process. However, in the present work, the increase of the proximity effect with decreasing size/increasing strain rather suggests that the Cu–Nb interfaces are less damaged or distorted than expected. Then, if some mechanical alloying arose during the severe plastic deformation process, the heat treatment performed at 600 °C at a diameter $d = 7.19$ mm may have cleaned the thermodynamically unstable Cu–Nb mixed zones by solid-state diffusion, restoring mono-atomic regions, as observed on other samples after annealing at 300 °C [7, 9]. Further drawing to obtain the present samples would have then only lead to the build-up of clean semi-coherent Cu–Nb interfaces (with misfit dislocations), as observed prior to the formation of alloyed interfaces [28].

In our previous works, we have investigated the annealing effects on the microstructure and magnetic properties of a Cu–15% Nb composite, with niobium filaments in the micrometre scale [17–19]. High annealing temperature led to spheroidization followed by coarsening of the niobium constituents [29]. As both the annealing temperature and time were increased, the coarsening became the predominant mechanism contributing to the coupling between the niobium filaments. In consequence, there was an increase in size of the niobium phase, in addition to a suppression of tiny normal regions which, upon cooling to low temperatures, could become weak superconducting elements due to the proximity effect. A double-peak structure in the $M(H)$ curves was also observed. In consequence of the increasing coarsening, the low-field peak was seriously suppressed, while the second peak was enhanced [17–19]. A direct comparison of the magnetization data with SEM images revealed that the structural distortion of the Cu–Nb interfaces was the cause of the strong suppression of the proximity effect, and consequently of the first magnetization peak [19]. In addition, it was observed that enhanced coarsening of niobium filaments leads to an increase in the second magnetization peak [17–19], despite a possible contribution from the gradual recrystallization of Nb.

A comparison between the experimental data on the annealed Cu–Nb *microcomposite* [17–19] and the present heavily deformed Cu–Nb *nanocomposites* suggests that the magnitude of the second magnetization peak is mainly sensitive to the thickness of the niobium, a conclusion that agrees with the simple phenomenological model discussed above. As a final comment, we have to note that the double-peak structure disappears in the descending branch of the $M(H)$ curves (see figure 4(a)). The same behaviour was observed for the annealed Cu–Nb microcomposites [17–19]. The three main mechanisms of irreversibility, bulk pinning, surface barriers and geometrical barriers, act in drastically different ways when the applied field increases compared to when it decreases [30–34]. As discussed in [19], it is believed that the complicated interplay of these irreversibility mechanisms obscures the double-peak structure in the descending branch of the $M(H)$ curves.

4. Conclusions

In summary, we have presented a study of the influence of applied strain via cold drawing on the superconducting properties for a series of Cu–3.5% Nb nanocomposite wires, containing nanometre-scale (below 10 nm) Nb filaments, embedded in a nanometre-size Cu matrix, with interfilamentary distance below 2 nm. The increasing strain leads to only minor modifications of the superconducting critical temperature of the system. Also, no major differences regarding the H_{c2} data were observed among the investigated conductors. However, the main difference is the shape of the DC magnetization curves. Notably, the investigated samples exhibit a double-peak structure in the ascending branch of the magnetization curves. The first peak, which occurs at low magnetic fields, is related to the superconducting proximity effects in the Cu matrix and is enhanced as the interfilamentary spacing d_{Cu-0} decreases, as expected. In an opposite manner, the second peak is almost suppressed as the dimension of Nb filaments d_{Nb} decreases, a fact suggesting that the second peak is related mainly to the size of the niobium filaments. A simple phenomenological concept has been proposed in order to explain the basic experimental observations.

Acknowledgments

This work was partially supported by FAPESP, CAPES-DAAD, CNPq and FAPERJ.

References

[1] Bevk J, Harbison K J P and Bell J L 1978 *J. Appl. Phys.* **49** 6031
[2] Pantsyrnyi V I 2002 *IEEE Trans. Appl. Supercond.* **12** 1189
[3] Awaji S, Watanabe K and Katagiri K 2003 *Supercond. Sci. Technol.* **16** 1059
[4] Thilly L, Lecouturier F, Coffe G, Peyrade J P and Askénazy S 2000 *IEEE Trans. Appl. Supercond.* **10** 1269
[5] Thilly L, Lecouturier F and von Stebut J 2002 *Acta Mater.* **50** 5049
[6] Raabe D and Hangen U 1995 *J. Mater. Res.* **10** 3050
[7] Sauvage X, Renaud L, Deconihout B, Blavette D, Ping D H and Hono K 2001 *Acta Mater.* **49** 389
[8] Raabe D, Heringhaus F, Hangen U and Gottstein G 1995 *Z. Metallkd.* **86** 405
[9] Sauvage X, Thilly L, Lecouturier F, Guillet A and Blavette D 1999 *Nanostruct. Mater.* **11** 1031
[10] Hangen U and Raabe D 1995 *Phys. Status Solidi* a **147** 515
[11] Heringhaus F, Schneider-Muntau H and Gottstein G 2003 *Mater. Sci. Eng.* A **347** 9
[12] Klein J D and Rose R M 1990 *J. Appl. Phys.* **67** 930
[13] Dubey S S, Dheer P N, Reddy Y S, Krishna M M and Sharma R G 1999 *Mater. Sci. Eng.* B **60** 118
[14] Raabe D and Heringhaus F 1994 *Phys. Status Solidi* a **142** 473
[15] Raabe D and Mattissen D 1999 *Acta Mater.* **47** 769
[16] Sandim M J R, Sandim H R Z, Bernardi H H, Shigue C Y, das Virgens M G, Ghivelder L, Awaji S, Watanabe K and Iwaki G 2005 *Supercond. Sci. Technol.* **18** 35
[17] Sandim M J R, Sandim H R Z, Shigue C Y, Filgueira M and Ghivelder L 2003 *Supercond. Sci. Technol.* **16** 307
[18] Sandim M J R, Sandim H R Z, Stamopoulos D, Renzetti R A and Ghivelder L 2005 *Supercond. Sci. Technol.* **18** 1151
[19] Stamopoulos D, Pissas M, Sandim M J R and Sandim H R Z 2006 *Physica* C **442** 45
[20] Takahashi S and Tachiki M 1986 *Phys. Rev.* B **33** 4620
[21] Sidorenko A, Sürgers C, Trappmann T and v Löhneysen H 1996 *Phys. Rev.* B **53** 11751
[22] Krasnov V M, Kovalev A E and Oboznov V A 1996 *Phys. Rev.* B **54** 15448
[23] Carty G J, Machida M and Hampshire D P 2005 *Phys. Rev.* B **71** 144507
[24] Vidal V, Thilly L, Lecouturier F and Renault P-O 2006 *Acta Mater.* **54** 1063
[25] Vidal V, Thilly L, Lecouturier F and Renault P-O 2006 *Mater. Sci. Eng.* A submitted
[26] Hosford W F 1964 *Trans. TMS AIME* **230** 12
[27] Funkenbusch P D and Courtney T H 1985 *Acta Metall.* **33** 913
[28] Dupouy F, Snoeck E, Casanove M J, Roucau C, Peyrade J P and Askénazy S 1996 *Scr. Mater.* **34** 1067
[29] Raabe D and Ge J 2004 *Scr. Mater.* **51** 915
[30] Nideröst M, Frassanito R, Saalfrank M, Mota A C, Blatter G, Zavaritsky V N, Li T W and Kes P H 1998 *Phys. Rev. Lett.* **81** 3231
[31] Pissas M and Stamopoulos D 2001 *Phys. Rev.* B **64** 134510
[32] Lyard L *et al* 2004 *Phys. Rev.* B **70** 180504(R)
[33] Liang R, Bonn D A, Hardy W N and Broun D 2005 *Phys. Rev. Lett.* **94** 117001
[34] Morozov N, Zeldov E, Konczykowski M and Doyle R A 1997 *Physica* C **291** 113